JOURNAL OF GEOPHYSICAL RESEARCH, VOL. 100, NO. C7, PAGES 13,279–13,294, JULY 15, 1995

In situ phytoplankton absorption, fluorescence emission, and particulate backscattering spectra determined from reflectance

Collin S. Roesler[1] and Mary Jane Perry
School of Oceanography, University of Washington, Seattle

Abstract. An inverse model was developed to extract the absorption and scattering (elastic and inelastic) properties of oceanic constituents from surface spectral reflectance measurements. In particular, phytoplankton spectral absorption coefficients, solar-stimulated chlorophyll *a* fluorescence spectra, and particle backscattering spectra were modeled. The model was tested on 35 reflectance spectra obtained from irradiance measurements in optically diverse ocean waters (0.07 to 25.35 mg m^{-3} range in surface chlorophyll *a* concentrations). The universality of the model was demonstrated by the accurate estimation of the spectral phytoplankton absorption coefficients over a range of 3 orders of magnitude (ρ = 0.94 at 500 nm). Under most oceanic conditions (chlorophyll *a* < 3 mg m^{-3}) the percent difference between measured and modeled phytoplankton absorption coefficients was <35%. Spectral variations in measured phytoplankton absorption spectra were well predicted by the inverse model. Modeled volume fluorescence was weakly correlated with measured chl *a*; fluorescence quantum yield varied from 0.008 to 0.09 as a function of environment and incident irradiance. Modeled particle backscattering coefficients were linearly related to total particle cross section over a twentyfold range in backscattering coefficients (ρ = 0.996, n = 12).

1. Introduction

The trend in biological oceanography toward noninvasive methods for determining phytoplankton biomass and primary production has stimulated new developments in the in situ measurement of optical characteristics of phytoplankton such as absorption and fluorescence. Interest in carbon cycling has lead to renewed interest in quantifying the concentration of organic particles in the ocean. Noninvasive in situ techniques that can be applied to data collected by satellite or aircraft are particularly important for addressing the role of phytoplankton and carbon in global climate change. The light emanating from the surface of the ocean contains a wealth of information regarding the absorption and scattering (elastic and inelastic) processes by the water itself and by the dissolved and particulate constituents contained within the water. It is not surprising therefore that measurements of the irradiance reflectance can provide information about these processes if the contributions to absorption and scattering can be separated into useful components.

The phytoplankton spectral absorption coefficient is an important parameter in bio-optical modeling of phytoplankton ecology. Many models of primary production depend upon estimates of photon absorption by phytoplankton (see review by *Bidigare et al.* [1992]). In addition, the spectrum of the phytoplankton absorption coefficient provides information on the pigment composition (and possibly taxonomy) [*Yentsch*, 1962; *Bidigare et al.*, 1989] and physiological states such as photoadaptation [*Neori et al.*, 1984] and nutrient stress [*Heath et al.*, 1990]. Although phytoplankton absorption coefficients can be measured for samples concentrated on filter pads with a correction for path length amplification [*Yentsch*, 1962; *Kiefer and SooHoo*, 1982; *Mitchell and Kiefer*, 1984, 1988; *Kishino et al.*, 1985; *Yentsch and Phinney*, 1989, 1992; *Mitchell*, 1990], noninvasive methods typically rely on correlation between chlorophyll *a* (chl *a*) (see notation section for additional abbreviations and symbols) concentrations and reflectance ratios for selected wavelengths [*Gordon and Morel*, 1983]. In situ multispectral instrumentation is currently available for determining total absorption coefficients [*Zaneveld et al.*, 1992; *Moore et al.*, 1992; *Bricaud et al.*, 1995]. However, these measurements also require inverse models to extract the contribution by phytoplankton from the total absorption coefficient [*Roesler et al.*, 1989; *Roesler and Zaneveld*, 1994].

Solar-stimulated or natural fluorescence of chl *a* has been shown to be correlated with both chl *a* concentration and phytoplankton production, although the exact relationship to primary production is not well understood [*Falkowski and Kiefer*, 1985; *Chamberlin et al.*, 1990; *Chamberlin and Marra*, 1992; *Kiefer and Reynolds*, 1992; *Stegmann et al.*, 1992]. Methods for the estimation of solar-stimulated fluorescence from reflectance or upward radiance typically require simplifying assumptions to be made about the character of the backscattering, reflectance, and/or fluorescence spectra. For example, radiance or reflectance measured at 683 nm is corrected for backscattered photons by assuming a constant backscattering coefficient [*Chamberlin et al.*,

[1]Now at Department of Marine Sciences, University of Connecticut, Groton.

Paper number 95JC00455.
0148-0227/95/95JC-00455$05.00

1990], a constant attenuation coefficient at 683 nm [*Kitchen and Pak*, 1987; *Stegmann et al.*, 1992], or a constant slope in the radiance (or reflectance) about the fluorescence wave band (e.g., 650 to 710 nm) [*Neville and Gower*, 1977; *Kishino et al.*, 1984b; *Sugihara et al.*, 1986]. An alternative approach is to assume that the fluorescence spectrum has a Gaussian wavelength dependence and then to apply best fit parameters to measured reflectance or upward radiance or reflectance spectra to separate the fluorescence signal [*Gordon*, 1979; *Topliss*, 1985; *Kishino et al.*, 1986].

The scattering of photons, unlike absorption, does not result in photon annihilation, but simply, photon redirection. In the ocean, particles of varying sizes and indices of refraction as well as density fluctuations in the water itself are responsible for the scattering. The magnitude of the scattering or backscattering coefficient can provide estimates of total suspended matter, analogous to the relationships established for transmissometers [*Bishop*, 1986]. Inversion of the scattering spectrum can be used to predict the size distribution of the suspended particles [*Shifrin*, 1988].

This paper describes a model whereby phytoplankton absorption spectra, solar-stimulated chl *a* fluorescence emission spectra, and total backscattering spectra can be determined from in situ measurements of spectral irradiance or remotely sensed reflectance without constraining the spectral variability. The solution is based upon the spectral reflectance mixture model of *Adams et al.* [1986] and *Johnson et al.* [1983]. In their approach there exists a library or set of reflectance spectra for individual minerals. The nondimensional shape of the reflectance spectrum for each mineral is defined as its basis vector; the product of a mineral's basis vector and its concentration specifies the actual reflectance spectrum of the mineral. The total measured reflectance spectrum then can be expressed as a linear combination of the products of the basis vectors (relative reflectance shapes) and the abundances of the minerals present. This approach has been used to determine mineral composition and concentration from remotely sensed spectra [*Adams et al.*, 1993; *Johnson et al.*, 1992]. In the ocean the inherent optical properties are the fundamental parameters determining reflectance spectra as specified by the radiative transfer equation. Thus the absorption and backscattering coefficients can be defined as products of their basis vectors and their magnitudes. Although this approach is similar to others [*Morel and Prieur*, 1977; *Sugihara et al.*, 1985; *Gordon et al.*, 1988], the mixture model presented here explicitly takes advantage of the spectral information in the basis vectors and measured reflectances.

2. Field Methods

Near-surface water samples and optical measurements were collected on a series of cruises from a wide range of optical domains (Table 1). Optical measurements were made at approximately local noon just prior to and/or immediately following water collection in order to minimize variations in solar angle (see section 3).

2.1. Water Analyses

Chl *a* concentrations were determined from water samples filtered onto glass fiber filters (Whatman GF/F, nominal pore size 0.7 μm) and extracted in 90% acetone for at least 48 hours at −40°C. Samples were then sonicated for 7 min and centrifuged prior to fluorometric analysis [*Holm-Hansen et al.*, 1965].

Optical density spectra of particulate samples concentrated onto GF/F filters were measured on a SLM-Aminco DW-2C dual-beam spectrophotometer. When possible, water samples were stored on ice in the dark and processed in the laboratory within hours of collection. Otherwise, the processed filters were stored in liquid nitrogen to minimize pigment degradation (R. F. Davis, personal communication, 1989). Optical density spectra of the particulate material were measured on the filter before and after methanol extraction, respectively. Hot methanol was used to remove the chlorophylls and carotenoids [*Kishino et al.*, 1985]; this method was modified by the addition of a hot water extraction for removal of phycobilipigments [*Roesler*, 1992]. The material remaining on the filter was tripton, including all living and dead particulate material exclusive of the extracted pigments. Spectral absorption coefficients were calculated from optical density spectra

$$a(\lambda) = \frac{2.303\mathrm{OD}(\lambda)}{L} 100 \tag{1a}$$

$$L = \frac{V}{A}\beta \tag{1b}$$

where 2.303 is the transform from $\log_{10}$ to $\log_e$, OD(λ) is the measured optical density corrected for the baseline signal with a blank filter pad, L is the optical path length, V is the volume of sample filtered (milliliters), A is the effective area of the filter (square centimeters), β is a spectrally weighted path length amplification factor associated with scattering by the filter pad [*Roesler*, 1992], and 100 is the conversion from centimeters to meters. The difference between the total particulate and the tripton absorption spectra is that component due to the solvent-extractable phytoplankton pigments as they were in situ, i.e., the phytoplankton absorption spectrum $a_\phi(\lambda)$. Absorption by the dissolved organic component of seawater (gelbstoff) was determined from (1a) where the optical density spectrum was measured on the GF/F filtrate in 10-cm quartz cuvettes and L = 0.1 m. No corrections for scattering by particles <0.7 μm in diameter were made, as there was negligible offset from zero in the OD spectrum at red wavelengths.

Particle concentrations and size distributions were determined using a Coulter counter with multisizer accessory. Water samples of volume 0.5, 2.0, and 50 mL were analyzed with aperture diameters of 30, 100, and 400 μm, respectively, enabling the accurate determination of particles with equivalent spherical diameters (ESD) of 2 to 200 μm. Filtered seawater (0.2-μm Nuclepore) from each site was used as a blank correction for each sample. Standard Coulter beads of diameter 5.11, 20.31, and 42.34 μm were used for daily calibration. Total geometric cross-sectional area σ was determined from

$$\sigma = \sum_{d=2}^{200} N(d)\,\frac{\pi}{4}\,d^2 \tag{2}$$

at 1-μm increments, where $N(d)$ is the concentration of particles with an ESD of d.

Table 1. Site Information and Optical Data for Each Sample

Site	Latitude, Longitude, °N, °W	Date	chl a, mg m^{-3}	a_ϕ, m^{-1}	a_{tg}, m^{-1}	$\hat{R}_F(683)$	$\hat{R}(683)$	$\hat{b}_{bT}(683)$, m^{-1}
			Estuarine Environment					
Puget Sound	48, 123	April 1991	7.34	0.0839	0.1101	0.00216	0.0025	0.0039
		May 1991	11.39	0.0795	0.1207	0.00484	0.0061	0.0102
		June 1991	7.84	0.0256	0.0914	0.00246	0.0027	0.0043
			7.84	0.0256	0.0914	0.00160	0.0010	0.0018
			5.21	0.0505	0.0589	0.00399	0.0181	0.0283
		Aug. 1991	4.89	0.0226	0.1137	0.00228	0.0092	0.0141
			4.89	0.0223	0.1136	0.00124	0.0052	0.0081
			8.72	0.0751	0.1111	0.00260	0.0025	0.0039
			8.72	0.0751	0.1111	0.00246	0.0022	0.0036
		Sept. 1991	25.34	0.1670	0.0830	0.00469	0.0036	0.0067
			25.35	0.1672	0.0831	0.00311	0.0045	0.0070
			Fjord Environment					
Dabob Bay	48, 124	April 1990	1.85	0.0183	0.0908	0.00062	0.0030	0.0053
			2.00	0.0107	0.0881	0.00059	0.0031	0.0058
			1.71	0.0121	0.0806	0.00122	0.0044	0.0065
		June 1990	1.45	0.0095	0.0846	0.00095	0.0026	0.0038
			1.59	0.0099	0.0850	0.00064	0.0028	0.0040
			1.47	0.0096	0.1072	0.00044	0.0035	0.0053
			1.32	0.0103	0.0770	0.00045	0.0022	0.0032
			1.25	0.0139	0.1264	0.00046	0.0025	0.0036
			Coastal Environment					
Gulf of Maine	43, 69	July 1990	2.79	0.0370	0.0392	0.00060	0.0014	0.0021
			2.79	0.0367	0.0390	0.00052	0.0009	0.0014
			1.29	0.0228	0.0123	0.00053	0.0013	0.0020
			0.68	0.0097	0.0182	0.00071	0.0022	0.0033
			0.52	0.0099	0.0209	0.00035	0.0019	0.0028
	44, 68		0.55	0.0138	0.0146	0.00068	0.0023	0.0040
			0.51	0.0119	0.0783	0.00016	0.0017	0.0027
			0.51	0.0119	0.0783	0.00039	0.0014	0.0026
Oregon coast	42, 128	Sept. 1991	0.50	0.0196	0.0124	0.00085	0.0005	0.0008
	45, 125		0.63	0.0190	0.0257	0.00053	0.0012	0.0019
			1.18	0.0190	0.0257	0.00060	0.0012	0.0019
	45, 124		1.10	0.0202	0.0090	0.00096	0.0007	0.0013
			Oceanic Environment					
Oregon coast	42, 132	Sept. 1991	0.07	0.0026	0.0034	0.00033	0.0002	0.0007
			0.09	0.0025	0.0048	0.00028	0.0003	0.0007
			0.09	0.0026	0.0055	0.00019	0.0004	0.0003
			0.09	0.0029	0.0058	0.00014	0.0003	0.0006

Variables are chl a, chlorophyll a; a_ϕ and a_{tg}, measured absorption coefficients for phytoplankton ϕ and tripton/gelbstoff components, respectively, averaged over photosynthetically available radiation; $\hat{R}_F(683)$, modeled reflectance due to chl a fluorescence at 683 nm; $\hat{R}(683)$, modeled reflectance at 683 nm without the influence of fluorescence; and $\hat{b}_{bT}(683)$, modeled total backscattering coefficient at 683 nm.

2.2. Irradiance Measurements

An integrated optical profiling system was used to measure above-water downward, in-water upward, and in-water downward vector spectral irradiance (LiCor UW1800). The package was also equipped with depth (Foxboro 1125) and tilt sensors (AccuStar 02383-09). Irradiance spectra measured with >2° tilt relative to the vertical were discarded. Spectral irradiance was collected at 1-nm resolution over the range 390 to 750 nm with a 5-nm band pass. Downward vector photosynthetically available radiation (PAR) (LiCor LI190) was continuously monitored from the highest point on the vessel and was used to correct the in-water measurements for variations in solar irradiance during and between scans. In-water scans for which the variation in surface PAR was >5% were discarded.

Waves and swells necessitated measurement of all spectra a small distance below the surface to prevent sensor emergence. Focusing and defocusing of downward irradiance onto the sensor by waves and ripples resulted in noisy downward irradiance spectra. Hence it was necessary to model downward spectral irradiance just beneath the surface, $\hat{E}_d(\lambda, z_{0-})$, from the downward irradiance measured just above the sea surface, $E_d(\lambda, z_{0+})$:

$$\hat{E}_d(\lambda, z_{0-}) = \tau E_d(\lambda, z_{0+}) \tag{3a}$$

where τ is the transmission across the interface. Transmission is highly dependent upon solar angle, wind speed, and wave height and was determined uniquely for each set of irradiance profiles in the following manner. Downward irradiance spectra were measured at two depths in the near-surface waters, z_1 and z_2, such that $z_2 > z_1$ and z_1 was sufficiently deep to prevent the instrument from emerging (approximately 10 to 30 cm below the largest wave trough). A 30-nm wavelength range was selected in the region of minimal attenuation in the water, $\Delta\lambda_{min}$; this range varied as a function of water type and was different for every location.

The spectrally averaged attenuation coefficient over $\Delta\lambda_{min}$ was calculated from the two downward irradiance spectra averaged over $\Delta\lambda_{min}$

$$k_d(\Delta\lambda_{min}) = -\frac{1}{z_2 - z_1} \ln \frac{E_d(\Delta\lambda_{min}, z_2)}{E_d(\Delta\lambda_{min}, z_1)}. \quad (3b)$$

This attenuation coefficient, calculated over the interval z_1 to z_2, was then used to determine the magnitude of the downward irradiance at z_{0-} from the measured irradiance at z_1, averaged over $\Delta\lambda_{min}$:

$$\hat{E}_d(\Delta\lambda_{min}, z_{0-}) = E_d(\Delta\lambda_{min}, z_1) \exp [k_d(\Delta\lambda_{min}) z_1]. \quad (3c)$$

Thus the transmission across the interface was determined at $\Delta\lambda_{min}$

$$\tau(\Delta\lambda_{min}) = \frac{\hat{E}_d(\Delta\lambda_{min}, z_{0-})}{E_d(\Delta\lambda_{min}, z_{0+})}. \quad (3d)$$

Setting $\tau = \tau(\Delta\lambda_{min})$ for all wavelengths, $\hat{E}_d(\lambda, z_{0-})$ was then calculated from (3a). This approach assumes that $k_d(\Delta\lambda_{min})$, calculated over z_1 to z_2, is representative of the interval z_{0-} to z_1 and that the transmission across the air/sea interface is independent of wavelength. Errors associated with the first assumption are minimized by reducing the distance between z_{0-} and z_2 [*McCormick*, 1992]. The second assumption was tested in Puget Sound on a very calm day under conditions of no wind and flat sea surface. $E_d(\lambda, z_{0-})$ was measured directly ($z_{0-} < 10$ cm) and was compared to $\hat{E}_d(\lambda, z_{0-})$, the calculated spectral values; the modeled and measured spectra were indistinguishable.

Upward irradiance spectra were not affected by surface processes, hence $\hat{E}_u(\lambda, z_{0-})$ was calculated for the entire spectrum by replacing $\Delta\lambda_{min}$ with all λ in (3b) and (3c) and using measurements of upward spectral irradiance at z_1 and z_2. Subsurface irradiance reflectance was calculated from the ratio of upward to downward spectral irradiance (see section 3).

3. Reflectance Theory

The in situ spectral irradiance reflectance in the ocean at a depth z is defined as

$$R(\lambda, z) \equiv \frac{E_u(\lambda, z)}{E_d(\lambda, z)} \quad (4)$$

where λ is wavelength and E_u and E_d are the in situ upward and downward spectral quantum irradiances measured at z. The radiative transfer equation, which relates the light field in the water column to the absorption and scattering coefficients inherent to the water column, is used to derive the relationship between reflectance and the inherent optical properties. Using a two-stream approximation (separating the light field into upward and downward components), *Zaneveld* [1982] derived an exact expression for the remote sensing reflectance R_{RS} defined as the ratio of upward radiance to downward irradiance measured just above the ocean surface

$$R_{RS} \equiv \frac{L_u}{E_d} = \frac{f_b b_{bT}}{2\pi(k + c - b_f f_L)} \quad (5)$$

where f_b is the radiance shape factor defined as the integrated backscattered downward radiance scaled to the backscattered downward scalar irradiance, b_{bT} is the total backscattering coefficient, k is the attenuation coefficient for nadir radiance, c is the beam attenuation coefficient, b_f is the forward scattering coefficient, f_L is the radiance shape factor defined as the integrated forward scattered upward radiance scaled to the total forward scattered radiance, and all optical terms are spectrally dependent.

Approximations by *Zaneveld* [this issue] to this exact solution indicate that the in situ reflectance determined just beneath the sea surface z_{0-} can be expressed in terms of the absorption and backscattering coefficients

$$R(z_{0-}) = \frac{Q}{2\pi\bar{\mu}_d(1 + \bar{\mu}_\infty)} \frac{b_{bT}}{a_T} \quad (6a)$$

where Q is the ratio of the upward irradiance to the upward radiance, $\bar{\mu}_d$ is the average cosine of the downward irradiance, b_{bT} is the total backscattering coefficient, a_T is the total absorption coefficient, and $\bar{\mu}_\infty$ is the average cosine of the asymptotic irradiance field. If Q is approximately 5.4 [*Austin*, 1974] and $\bar{\mu}_d$ and $\bar{\mu}_\infty$ vary from 0.5 to 1 (and $\bar{\mu}_\infty \leq \bar{\mu}_d$), the in situ reflectance in (6a) can be estimated by

$$\hat{R}(z_{0-}) = G \frac{b_{bT}}{a_T} \quad (6b)$$

where $\hat{R}$ is the estimated reflectance and G varies from 0.29 to 0.57 depending upon the angular dependence of the light field. Successive order scattering methods [*Morel and Prieur*, 1977] and Monte Carlo simulations [*Gordon et al.*, 1975; *Kirk*, 1984] result in the same expression, where G is approximately 0.33 for zenith Sun or 0.37 for uniform sky, dependent upon the average cosine of the incident photons just below the surface. The statistical expressions for G derived from the simulations are consistent with the range derived from the approximations (6a) to the exact solution (5).

The total absorption and backscattering coefficients can be expressed as the sum of the absorption and backscattering coefficients for all of the components in seawater. These, in turn, can further be expressed as the product of the magnitude and spectral shape of each component's absorption and backscattering coefficients

$$a_T(\lambda) = \sum_{i=1}^{I} a_i(\lambda) = \sum_{i=1}^{I} M_i \mathbf{a}_i(\lambda) \quad (7a)$$

$$b_{bT}(\lambda) = \sum_{j=1}^{J} b_{bj}(\lambda) = \sum_{j=1}^{J} M_j \mathbf{b}_{bj}(\lambda) \quad (7b)$$

where a_T and b_{bT} are the total absorption and backscattering coefficients for natural seawater, a_i and b_{bj} are the absorption and backscattering coefficients for components i and j($i = 1, I$ and $j = 1, J$ are the complete set of components in seawater that absorb and backscatter, respectively), M_i and M_j are the magnitudes of the absorbing and backscattering coefficients, and $\mathbf{a}_i(\lambda)$ and $\mathbf{b}_{bj}(\lambda)$ are the dimensionless basis vectors of the absorption and backscattering spectra (spectral shapes) for the ith and jth compo-

nents, respectively. Substitution of (7a) and (7b) into (6b) results in

$$\hat{R}(\lambda, z_{0-}) = G \frac{\sum_{j=1}^{J} M_j \mathbf{b}_{bj}(\lambda)}{\sum_{i=1}^{I} M_i \mathbf{a}_i(\lambda)} \quad (8)$$

which is the forward equation for determining irradiance reflectance from its components. Because phytoplankton is one of the components responsible for absorption, the phytoplankton spectral absorption coefficient can be derived by inversion of (8).

4. Model Development

4.1. The Forward Expression for Reflectance

The first steps in the development of the forward equation (8) were to select a minimal set of components to adequately parameterize the reflectance and to define the wavelength dependence of their basis vectors. Previous studies of absorption have shown that the dominant absorbing materials in natural ocean waters are water itself, phytoplanktonic pigments, tripton (often designated detritus, but which also includes the living particulate cellular material, exclusive of pigments, associated with phytoplankton, bacteria, and zooplankton), and gelbstoff (dissolved organic matter) [*Kirk*, 1980; *Prieur and Sathyendranath*, 1981; *Kishino et al.*, 1984a]. The total absorption coefficient can be approximated by

$$\hat{a}_T(\lambda) = a_w(\lambda) + a_\phi(\lambda) + a_t(\lambda) + a_g(\lambda) \quad (9)$$

where $\hat{a}_T$ is the estimated total absorption, and the subscripts w, ϕ, t, and g designate water, phytoplankton, tripton, and gelbstoff. The total absorption $\hat{a}_T$ is considered to be an estimate because one or more additional components may have been omitted from (9). For example, the contribution to absorption by inorganic particles is usually minor in most oceanic areas [cf. *Betzer et al.*, 1988] but may be more important in coastal and estuarine environments where sediment loads from rivers are significant. The spectral absorption coefficients for pure water $a_w(\lambda)$ were approximated by the absorption for clearest ocean water [*Smith and Baker*, 1981].

The absorption coefficients of the remaining components were broken into magnitude coefficients M_i, with units of m^{-1} and dimensionless basis vectors $\mathbf{a}_i(\lambda)$, which describe the spectral shape of the absorption spectra. The basis vector for phytoplankton absorption $\mathbf{a}_\phi(\lambda)$ can be difficult to constrain because of its dependence on pigment composition, concentration, and packaging [*Sathyendranath et al.*, 1987; *Bricaud et al.*, 1988]. Hence an average basis vector, derived from the spectral phytoplankton absorption coefficients from the San Juan Archipelago [*Roesler et al.*, 1989, Figure 3a] was used. The modeled phytoplankton absorption spectrum in (9) was then expressed as

$$\hat{a}_\phi(\lambda) = M_\phi \mathbf{a}_\phi(\lambda) \quad (10)$$

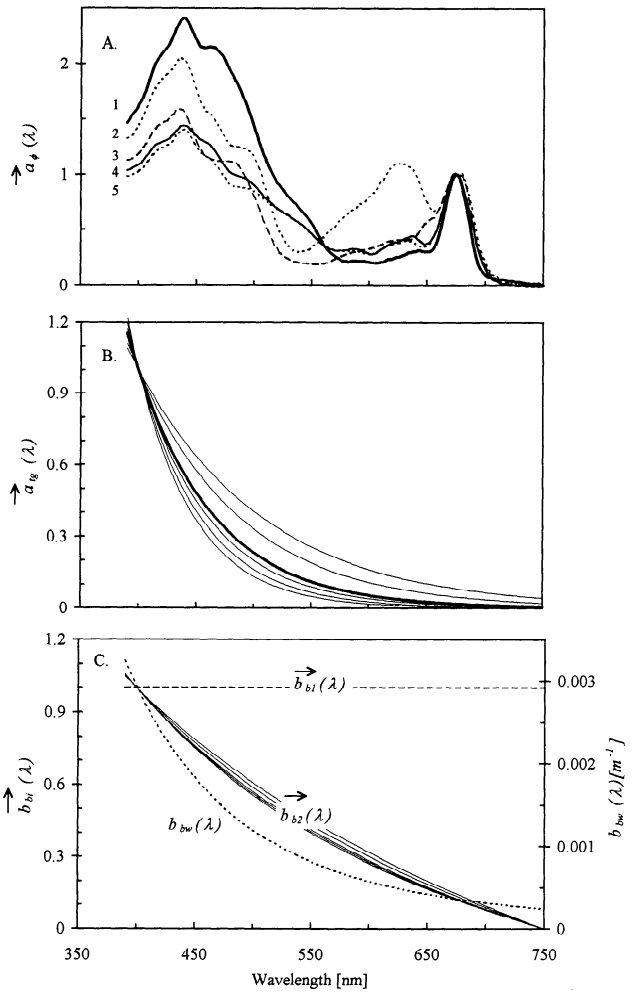

Figure 1. (a) Dimensionless phytoplankton absorption basis vector $\mathbf{a}_\phi(\lambda)$ determined from independent data published by *Roesler et al.* [1989]; spectrum labeled 1. Additional basis vectors used for sensitivity analysis of equation (14) were from pure cultures of *Synechococcus* sp. (labeled 2), *Dunaliella salina* (labeled 3), *Chaetoceros gracilis* (labeled 4), and *Amphidinium carterae* (labeled 5). (b) Dimensionless basis vector for tripton/gelbstoff absorption $\mathbf{a}_{tg}(\lambda) = \exp[-S(\lambda - 400\ \text{nm})]$, where the spectral slope $S = 0.0145$ (bold curve) from *Roesler et al.* [1989]. Values of S for sensitivity analysis were 0.009, 0.011, 0.0145, 0.016, 0.018, and 0.020 (curves from top to bottom). (c) Dimensionless basis vectors for the two components of particle backscattering defined by equation (13) $\mathbf{b}_{b1}(\lambda) = \lambda^0$ (dashed curve) and $\mathbf{b}_{b2}(\lambda) = \lambda^{-Y} - \lambda_{750}^{-Y}$. In the initial run, $Y \equiv 1$ was not a variable. The sensitivity analyses were performed with Y initialized with values of 0, 0.5, 0.75, 1.0, 1.1, 1.2 ($\mathbf{b}_{b2}(\lambda)$ curves from top to bottom for $Y = 0.5$ to 1.2, respectively). Backscattering by water $b_{bw}(\lambda)$ is shown for reference (dotted curve [*Smith and Baker*, 1981]), and the basis vectors are scaled to a value of 1.0 at 400 nm.

where M_ϕ defines the magnitude and $\mathbf{a}_\phi(\lambda)$ defines the spectral shape of the spectrum (Figure 1a). Sensitivity analyses are described in section 4.3, and comparisons with measured $a_\phi(\lambda)$ are given in section 5.3.

The absorption of both tripton and gelbstoff decays exponentially with wavelength. The shape of these exponential functions varies slightly as a function of the composition of

organic material [*Carder et al.*, 1989]; however, the relative invariance found over a wide range of ocean waters [*Roesler et al.*, 1989, Table 1] indicates that the two components can be combined and approximated accurately by a single exponential function

$$\hat{a}_{tg}(\lambda) = M_{tg}\mathbf{a}_{tg}(\lambda) \tag{11a}$$

where

$$M_{tg} = a_{tg}(400\text{ nm}) \tag{11b}$$

defines the magnitude of the absorption coefficient and

$$\mathbf{a}_{tg}(\lambda) = \exp\,[-S(\lambda - 400\text{ nm})] \tag{11c}$$

is the single dimensionless basis vector $\mathbf{a}_{tg}(\lambda)$ used to describe the relative shape of the spectral absorption coefficient of the tripton/gelbstoff component (Figure 1b). The slope of the exponential, $S = 0.0145$, was taken from *Roesler et al.* [1989], although the sensitivity of the model was evaluated over a range of S values (Figure 1B, 0.009 to 0.02).

The total spectral backscattering coefficient $b_{bT}(\lambda)$ was separated into contributions by water $b_{bw}(\lambda)$ and total particles $b_{bp}(\lambda)$

$$b_{bT}(\lambda) = b_{bw}(\lambda) + b_{bp}(\lambda). \tag{12}$$

Spectral backscattering coefficients for water were taken from *Smith and Baker* [1981], although they include all molecular backscattering processes by dissolved components (Figure 1c). In situ measurements of single-wavelength backscattering coefficients are relatively rare [*Petzold*, 1972; *Maffione et al.*, 1991; *Bricaud et al.*, 1995]; in situ spectral backscattering coefficients for a specific component are even more difficult to obtain. Theoretical analyses based upon Mie approximations for spherical particles in combination with laboratory measurements have led to the following conclusions concerning spectral backscattering coefficients for oceanic particles [*Stramski and Kiefer*, 1991]. Scattering efficiencies are strongly dependent upon the ratio of the particle diameter to the wavelength of light and on the relative index of refraction. Backscattering by a population of large polydispersed particles is approximately spectrally flat, in the absence of anomalous dispersion [*Zaneveld and Kitchen*, 1994]. As the size of the particles decreases and/or monodispersion is approached, increased variability in the spectral shape is observed [*Bricaud and Morel*, 1986; *Stramski and Morel*, 1990; *Morel and Ahn*, 1990, 1991; *Ahn et al.*, 1992]. Because there is a broad range of particle diameters, shapes, and concentrations in the ocean, the dispersion in size may tend to cancel any strong wavelength dependence. Backscattering by inorganic particles will be similar to that by organic particles of like size and shape, although the indices of refraction and hence the magnitude of the backscattering will be greater [e.g., *Ackleson et al.*, 1994].

In the absence of measurements of spectral backscattering coefficients for oceanic particles, an approximation is required. The total particulate backscattering spectrum in (12) was partitioned into contributions by populations of large polydispersed particles $\hat{b}_{b1}(\lambda)$ and by populations of smaller particles with a more monodispersed size distribution $\hat{b}_{b2}(\lambda)$ such that

$$\hat{b}_{bp}(\lambda) = \hat{b}_{b1}(\lambda) + \hat{b}_{b2}(\lambda) \tag{13a}$$

where

$$\hat{b}_{b1}(\lambda) = M_{b1}\mathbf{b}_{b1}(\lambda) = M_{b1}\lambda^{0} \tag{13b}$$

$$\hat{b}_{b2}(\lambda) = M_{b2}\mathbf{b}_{b2}(\lambda) = M_{b2}(\lambda^{-1} - \lambda_{750}^{-1}) \tag{13c}$$

where M_{b1} and M_{b2} determine the magnitudes of the backscattering coefficients. The basis vectors, $\mathbf{b}_{b1}(\lambda)$ and $\mathbf{b}_{b2}(\lambda)$, define the wavelength dependence of the backscattering; λ_{750} removes the offset from zero (Figure 1c). The wavelength dependence of individual particles will be quite different from this approximation; however, the contribution by individual particles is not the goal of this model. Thus the bulk backscattering spectrum defined by this approximation assumes that the backscattering coefficients for individual particles can be combined and adequately approximated by a linear combination of the two magnitude/basis vector products in (13b) and (13c). While this is not accurate mathematically, the practical application of this assumption is adequate for the observed range in spectral dependence of particle backscattering coefficients in the ocean. The sensitivity of the model to the choice of wavelength dependence in $\mathbf{b}_{b2}(\lambda)$ was tested (see section 4.3).

The full expression for the reflectance in (8), in terms of the component basis vectors defined in (10), (11), and (13), is

$$\hat{R}(\lambda, z_{0-}) = G\frac{b_{bw}(\lambda) + M_{b1}\lambda^{0} + M_{b2}(\lambda^{-1} - \lambda_{750}^{-1})}{a_w(\lambda) + M_{\phi}\mathbf{a}_{\phi}(\lambda) + M_{tg}\exp\,[-0.0145(\lambda - 400)]} \tag{14}$$

4.2. The Inverse Model

The coefficients defining the magnitudes of the absorption and backscattering basis vectors, M_i and M_j (where $i = \phi$, tg and $j = b1$, $b2$), were obtained from regression of (14) onto $R(\lambda, z_{0-})$, with $G = 0.33$, using the Levenberg-Marquardt method [*Press et al.*, 1986]. This resulted in a unique set of M_i and M_j coefficients that, in combination with the basis vectors, best describe each in situ $R(\lambda, z_{0-})$. The wavelength range used for the regression was 380 to 660 nm to avoid the region of chl *a* fluorescence (see below). The regression minimizes errors between the model, the right-hand side of (14), and the measured reflectance to arrive at best fit values of M_i and M_j. The modeled reflectance is then reconstructed for each site from the right-hand side of (14) with the site-specific values of M_i and M_j derived from the regression. This is the best fit modeled reflectance from the regression based upon minimized errors. However, minimized errors do not necessitate that the reconstructed reflectance will accurately predict the measured reflectance if the model is inappropriate. Deviations between the reconstructed model and measured reflectances, $\hat{R}(\lambda, z_{0-})$ and $R(\lambda, z_{0-})$, will arise if (1) (6b) is an inaccurate description of near-surface reflectance [cf. *Aas*, 1987; *Gordon et al.*, 1975]; (2) an incomplete set of components is used to approximate the total absorption and backscattering coefficients in (7a) and (7b); (3) the basis vectors are inaccurate representations of spectral shape of the component absorption and backscattering coefficients; and/or (4) other inelastic scattering sources are present.

Step 1: First-order estimation of the phytoplankton absorption spectrum $\hat{a}_\phi(\lambda)$. The first-order estimator of the phytoplankton spectral absorption coefficient $\hat{a}_\phi(\lambda)$ is determined from (10) with the value of M_ϕ obtained from the multiple regression of (14). This spectral shape of $\hat{a}_\phi(\lambda)$ is defined by the spectrum of the input phytoplankton absorption basis vector $\mathbf{a}_\phi(\lambda)$.

Step 2: Estimation of the chl *a* fluorescence spectrum. The expressions for the reflectance in (6) and (14) do not contain inelastic scattering source terms, while the in situ reflectance spectrum $R(\lambda, z_{0-})$ calculated from (4) with measured irradiances does contain these signals. The difference between the measured reflectance spectrum and the modeled reflectance spectrum (reconstructed from the input basis vectors and the M coefficients derived from the regression of (14)) for those wavelengths at which chl *a* fluoresces (λ_F = 660–730 nm) is the contribution of chl *a* fluorescence emission to reflectance $\hat{R}_F(\lambda_F, z_{0-})$

$$\hat{R}_F(\lambda_F, z_{0-}) = R(\lambda_F, z_{0-}) - \hat{R}(\lambda_F, z_{0-}). \quad (15)$$

Step 3: Second-order estimation of the phytoplankton absorption spectrum $\mathring{a}_\phi(\lambda)$. The wavelength dependence of phytoplankton absorption defined by the basis vector $\mathbf{a}_\phi(\lambda)$ describes an average case. However, the measured in situ phytoplankton absorption spectrum $a_\phi(\lambda)$ may exhibit variations in wavelength dependence from $\mathbf{a}_\phi(\lambda)$ as a function of pigment concentration, composition, and packaging. Theoretically, such variations appear in the in situ reflectance spectrum $R(\lambda, z_{0-})$. Thus deviations between the modeled reflectance $\hat{R}(\lambda, z_{0-})$ and the in situ reflectance $R(\lambda, z_{0-})$ may contain information related to the variations in phytoplankton spectral absorption. To examine this hypothesis, the second-order estimator for phytoplankton absorption $\mathring{a}_\phi(\lambda)$ was calculated by the inversion of (14), corrected for chl *a* fluorescence over the λ_F wave band, using the set of values of M derived from regression

$$\mathring{a}_\phi(\lambda) = G\,\frac{b_{bw}(\lambda) + M_{b1}\lambda^{0} + M_{b2}(\lambda^{-1} - \lambda_{750}^{-1})}{r(\lambda, z_{0-}) - \hat{R}_F(\lambda_F, z_{0-})} - a_w(\lambda)$$

$$- M_{tg}\exp[-0.0145(\lambda - 400)]. \quad (16)$$

This step of the model forces all of the deviations between $R(\lambda, z_{0-})$ and $\hat{R}(\lambda, z_{0-})$ over the range 390 to 660 nm to be included in the phytoplankton absorption spectrum. The inclusion of the deviations allows the phytoplankton absorption coefficients to vary spectrally from the initial basis vector $\mathbf{a}_\phi(\lambda)$ shown in Figure 1a over 390 to 660 nm. From 660 to 750 nm, $\mathring{a}_\phi(\lambda)$ does not vary spectrally from the basis vector nor from $\hat{a}_\phi(\lambda)$.

The utility of this inverse spectral mixture model can be assessed by (1) how accurately the phytoplankton spectral absorption coefficients are predicted from the inverse model in (16) and (2) how well the measured reflectance spectrum is reproduced by the reconstruction in (14).

4.3. Sensitivity Analysis of the Forward Model

The ability of the forward equation (14) to accurately reconstruct the in situ reflectance spectrum depends upon the correct selection of spectra for the basis vectors for absorption and backscattering. Unrealistic basis vectors lead to erroneous estimates of reflectance spectra or to variations in the estimated coefficients M_i and M_j. To assess the sensitivity, the basis vector for each component was allowed to vary spectrally, and the percent coefficients of variation (cv) in the derived phytoplankton and tripton/gelbstoff absorption and particle backscattering coefficients (M_i and M_j) were determined. The larger the coefficient of variation, the more sensitive is the model to the selection of the basis vector.

Alternative basis vectors for phytoplankton absorption were derived from monospecific phytoplankton cultures [*Roesler*, 1992]. The species were chosen to represent a broad range of accessory pigment compositions (Figure 1A) as follows: *Chaetoceros gracilis* (chl *c*, fucoxanthin), *Amphidinium carterae* (chl *c*, peridinin), and *Dunaliella salina* (chl *b*, lutein), *Synechococcus* sp. (phycobilipigments). The blue to red peak absorption ratios, $a_\phi(436)$:$a_\phi(676)$, which are indicative of variations in pigment composition and packaging ranged from approximately 1.4 to 2.0.

The exponential coefficient S defining the slope of the exponential basis vector for the tripton/gelbstoff absorption in (11c) was allowed to vary from 0.009 to 0.02 (Figure 1b). These values represent extreme ranges in slope calculated from the mean plus/minus standard deviations for published triton or gelbstoff absorption, respectively [*Roesler et al.*, 1989, Table 1].

The wavelength dependence of the particle backscattering spectrum was selected to be a linear combination of $\mathbf{b}_{b1}(\lambda)$ and $\mathbf{b}_{b2}(\lambda)$, where the basis vectors are defined by (13b) and (13c). This approximation implies that all wavelength dependences observed in the in situ particle backscattering coefficients can be adequately represented by the sum of the spectrally invariant component and the component whose spectral dependence is proportional to λ^{-1}. The sensitivity of the model to this approximation was tested by reparameterizing the spectrally varying basis vector in (13c) by

$$\mathbf{b}_{b2}(\lambda) = (\lambda^{-Y} - \lambda_{750}^{-Y}) \quad (17a)$$

where Y, defining the wavelength dependence, was also a coefficient determined by the regression (Figure 1c). Thus the total particle backscattering in (13a) was redefined for the sensitivity analysis as

$$\hat{b}_{bp}(\lambda) = M_{b1}\lambda^{0} + M_{b2}(\lambda^{Y} - \lambda_{750}^{-Y}). \quad (17b)$$

5. Results

5.1. Water Sample Analyses and Optical Measurements

The optical environments ranged from clear oceanic waters to turbid estuarine waters (Table 1). Surface chl *a* concentrations varied from 0.07 to 25.35 mg m^{-3}, and phytoplankton absorption coefficients varied over fiftyfold in magnitude. The efficiency of the phytoplankton absorption coefficient normalized to chl *a* concentration $a^*_\phi(\lambda)$ varied by a factor of 8 in the blue region of the spectrum among the environments sampled (Figure 2). The absorption coefficients of the tripton/gelbstoff component varied from 0.0034 m^{-1} in the oceanic waters off the Oregon coast to 0.1264 m^{-1} in Dabob Bay.

The measured spectral reflectances were variable in shape and magnitude (Figure 3). The magnitude of the reflectance was generally <0.025 except for a shallow bay in Puget Sound and in the oceanic waters off Oregon where maximal reflectance exceeded 0.04. The wavelength of maximal re-

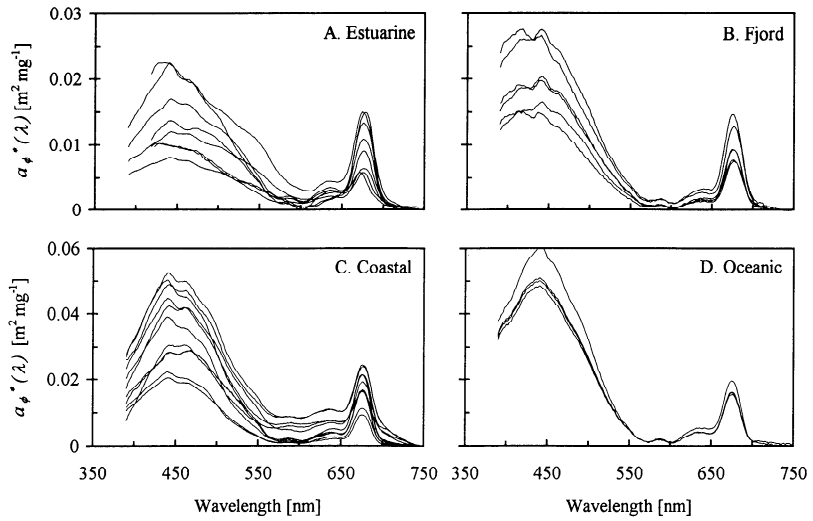

Figure 2. Measured chl a-specific phytoplankton absorption spectra $a^*_\phi(\lambda)$ for (a) estuarine, (b) fjord, (c) coastal, and (d) oceanic water types (see Table 1). Note different scales for Figures 2a and 2b versus 2c and 2d.

flectance was 440 nm in the oceanic waters, 490 nm in the coastal water, 540 nm in the fjord, and 565 nm in Puget Sound waters with very high chl a concentrations (>25 mg m^{-3}). The signature associated with solar-stimulated chl a fluorescence was evident in many of the spectra in the region about 683 nm.

5.2. Model Results: The Forward Equation

The irradiance reflectance $\hat{R}(\lambda, z_{0-})$ was reconstructed from (14) using magnitudes derived from the regression (section 4.2) for a set of samples with diverse magnitudes and spectral shapes (Figure 4). The shape of the modeled reflectance spectrum in the region 660 to 730 nm does not monotonically decrease but contains significant structure due to absorption and backscattering. In particular, the dip in the reflectance at 676 nm associated with chl a absorption is evident in the modeled reflectance spectrum from Puget Sound (labeled E in Figure 4). This absorption signature is not always apparent in the in situ reflectance spectrum $R(\lambda, z_{0-})$ due to the "filling in of the trough" by chl a fluorescence.

5.3. Model Results: The Inverse Model

First-order estimated spectral phytoplankton absorption coefficients $\hat{a}_\Phi(\lambda)$. The first-order estimation of the phytoplankton spectral absorption coefficients $\hat{a}_\phi(\lambda)$ is calculated from (10). These estimated coefficients were significantly correlated with the measured in situ coefficients a_ϕ at 436, 500, and 676 nm (ρ = 0.90, 0.92, and 0.92, respectively, n = 35; Figure 5) with rms error values of 0.166, 0.082, and 0.025, respectively. A linear regression between the two at 676 nm yielded a slope and intercept of 1.11 and −0.002, respectively, with an r^2 = 0.75. Four comparisons between the measured and estimated spectral absorption coefficients

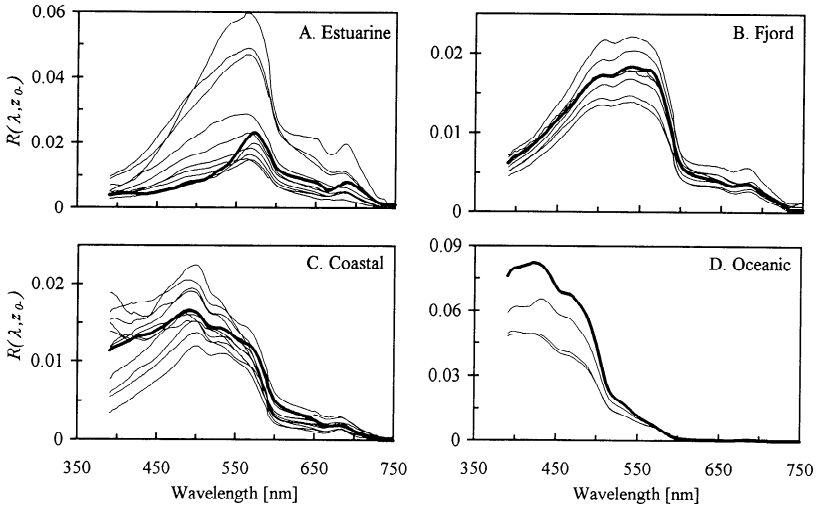

Figure 3. In situ spectral reflectance $R(\lambda, z_{0-})$ determined from measured irradiance spectra for (a) estuarine, (b) fjord, (c) coastal, and (d) oceanic water types. Bold spectra are shown in Figure 4. Note different scales for each water type.

are shown in Figure 6. The rms errors calculated over the entire spectrum were 0.0021, 0.0063, 0.0023, and 0.0007 for the four cases shown in Figures 6a through 6d, respectively. The magnitude of the estimation is reasonable, but the spectra are not identical, indicating that the basis vector is not adequate to describe the spectral dependence of the in situ phytoplankton absorption coefficient in all cases or waters.

Second-order estimated phytoplankton spectral absorption coefficients $\mathring{a}_\phi(\lambda)$. When the deviations between the modeled and in situ reflectances spectra were included in the estimated phytoplankton absorption spectra between 390 and 660 nm, the correlation between $\hat{a}_\phi(436)$ and measured $a_\phi(436)$ was slightly lower and the rms error slightly larger than for $\hat{a}_\phi(436)$ (Figure 5a; ρ = 0.87, rms = 0.180). However, $\mathring{a}_\phi(500)$ was a better predictor of $a_\phi(500)$ than $\hat{a}_\phi(500)$ (Figure 5b; ρ = 0.94, rms = 0.032). Because the deviations between estimated and in situ reflectance in the spectral region 660 to 730 nm were attributed by chl *a* fluorescence from (15), $\mathring{a}_\phi(\lambda_F) \equiv \hat{a}_\phi(\lambda_F)$. The additional signal incorporated in the second-order estimate served to reduced the rms error calculated over the entire spectrum (rms = 0.0029, 0.0055, 0.0020, and 0.0006 for Figures 6a through 6d) except in the estuarine case.

The sample averaged rms error calculated for all wavelengths was found to be lower for $\hat{a}_\phi$ than for $\mathring{a}_\phi$ (0.021 versus 0.029). However, when the estuarine samples were excluded from the analysis, the average rms error was lower for $\mathring{a}_\phi$ (0.008 versus 0.010 for $\hat{a}_\phi$). Overestimation of the phytoplankton absorption coefficient in the estuarine samples was a result of the significantly steeper exponential slopes in the tripton/gelbstoff absorption than were used in the model; measured S values approached 0.02. Excluding the estuarine samples, the average percent difference between $\mathring{a}_\phi$ and a_ϕ was 35%, with 18 of the 24 samples having <30% difference. In contrast, the average percent difference between $\hat{a}_\phi$ and a_ϕ was 59%, with 16 of the 24 samples exhibiting <30% difference.

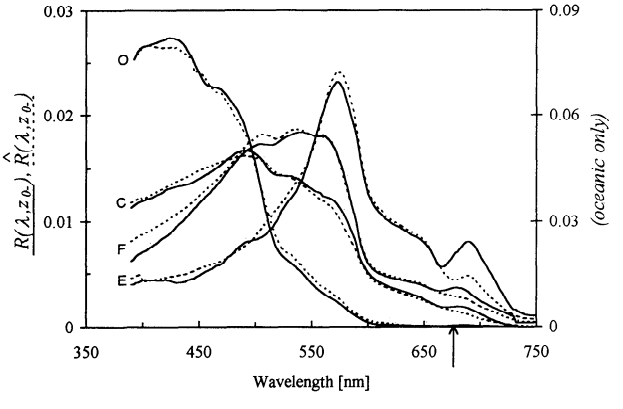

Figure 4. Comparison of in situ reflectance spectra $R(\lambda, z_{0-})$ (solid curve) with estimated spectra $\hat{R}(\lambda, z_{0-})$ (dashed curve) for estuarine (E), fjord (F), coastal (C), and oceanic (O) environments. The scale on the right-hand side refers to the oceanic spectrum only. Note the reflectance at 750 nm in E is not zero due to the very high backscattering coefficients. The difference between $R(\lambda, z_{0-})$ and $\hat{R}(\lambda, z_{0-})$ from 660 to 730 nm is the contribution to in situ reflectance by solar-stimulated chl *a* fluorescence $\hat{R}_F(\lambda, z_{0-})$. The arrow indicates 676 nm, the absorption peak associated with chl *a* that is predicted by the dip in reflectance by the model (most noticeable in spectrum E).

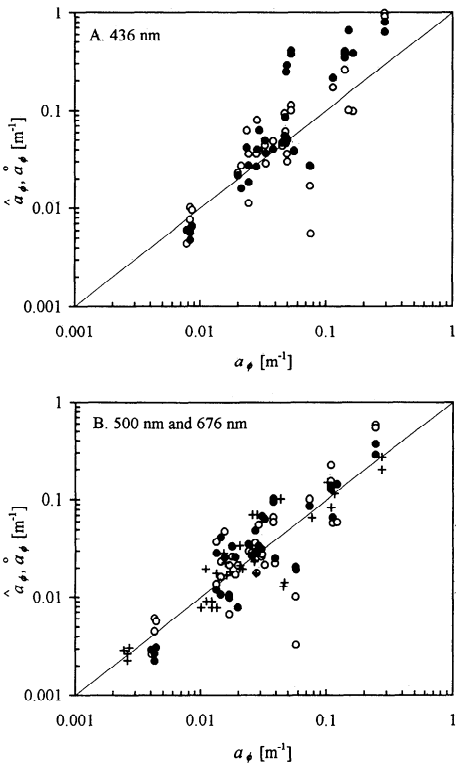

Figure 5. (a) First-order estimated $\hat{a}_\phi$ (open circles) or second-order estimated $\mathring{a}_\phi$ (solid circles) versus measured a_ϕ phytoplankton absorption coefficients at 436 nm. The solid line represents the 1:1 slope. (b) Same as Figure 5a, but for 500 nm; $\hat{a}_\phi$ at 676 nm are indicated by plus symbols.

The measured spectrum from the fjordal waters exhibits a broad peak over 410 to 440 nm, probably due to detrital pigments. The inclusion of this feature in the second-order estimate attests to the sensitivity of reflectance to absorption and attests to the sensitivity of the inverse model to spectral variations between in situ phytoplankton absorption and the input basis vector. In oceanic waters the slight differences between the large reflectance values measured and those derived from the expression in (14) were magnified in the extremely low phytoplankton absorption coefficients (Figure 6d).

Solar-stimulated chl *a* fluorescence spectra. The reflectance spectra associated with solar-stimulated chl *a* fluorescence showed some deviation from a Gaussian shape and exhibited significant variability in both the magnitude and shape (Table 1 and Figure 7). The wavelength of maximal fluorescence was shifted toward the infrared from 683 nm in many cases.

The scalar upward fluorescence emission $\hat{E}_{ouF}(\lambda_F)$ was modeled by scaling $\hat{R}_F(\lambda, z_{0-})$ to the downward spectral irradiance and to the average cosine of the upward light stream $\bar{\mu}_u$

$$\hat{E}_{ouF}(\lambda_F) = \frac{\hat{R}_F(\lambda_F, z_{0-})E_d(\lambda_F, z_{0-})}{\bar{\mu}_u}. \quad (18)$$

Fluorescence emission is isotropic, and thus the total fluorescence emission for the volume is twice the upward scalar emission. The spectrally integrated total volume fluores-

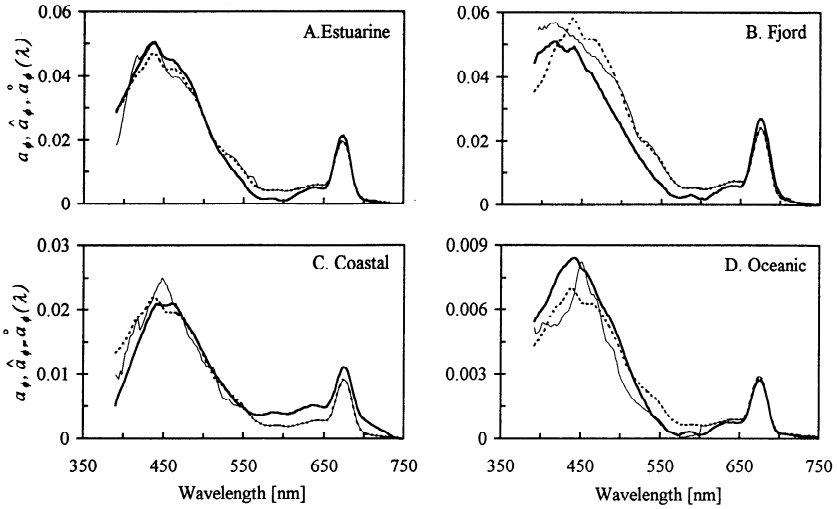

Figure 6. Examples of measured $a_\phi(\lambda)$ (bold curve), first-order estimated $\hat{a}_\phi(\lambda)$ (dotted curve), and second-order estimated $\mathring{a}_\phi(\lambda)$ (solid curve) spectral phytoplankton absorption from (a) estuarine, (b) fjord, (c) coastal, and (d) oceanic waters.

cence $\hat{F}$ was determined by using a value of 0.4 for $\bar{\mu}_u$ within the upper optical depth [*Kirk*, 1981] and integrating over λ_F. $\hat{F}$ varied from 0.03 to almost 5.0 μmol quanta m^{-3} s^{-1} and was linearly correlated with chl *a* concentration for all the samples, although significant variability existed within a water type (Figure 8a). No correlation is apparent between volume fluorescence and chl *a* concentration in the oceanic or estuarine waters, while in the coastal and fjordal waters there is a slight inverse correlation, although the trend is not significant.

The fluorescence quantum yield Φ (quanta fluoresced per quanta absorbed) was calculated from

$$\Phi = \frac{\hat{F}}{\int_{400}^{700} a_\phi(\lambda) E_d(\lambda) \bar{\mu}_d \, d\lambda} \tag{19}$$

where the product $E_d(\lambda)\bar{\mu}_d$ is the estimate of scalar downward spectral irradiance ($\bar{\mu}_d$ = 0.95 [*Kirk*, 1981]). Values of Φ ranged from 0.008 to 0.09. The maximal quantum yields for a given water type occurred at approximately 1000 μmol quanta m^{-2} s^{-1} surface irradiance, with yields tending to decrease at both lower and higher irradiances (Figure 8b).

Particulate backscattering coefficients. Total particulate backscattering coefficients were estimated from (13) using the model output values of M_{b1} and M_{b2} and the basis vectors $\mathbf{b}_{b1}(\lambda)$ and $\mathbf{b}_{b2}(\lambda)$ (Table 1). Although no independent measurements of particle backscattering coefficients were made, a strong correlation was found between the modeled spectrally integrated particle backscattering coefficient $\hat{b}_{bp}$ and σ, the total geometrical cross section for particles (ρ = 0.996, n = 12; Figure 9a). Over a twentyfold range of backscattering coefficients, σ was a better predictor

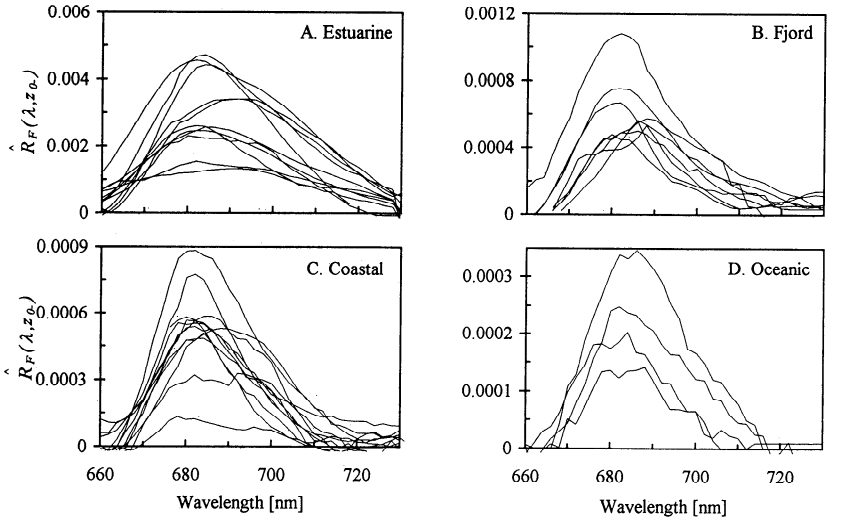

Figure 7. Reflectance spectra of solar-stimulated chl *a* fluorescence $\hat{R}_F(\lambda, z_{0-})$ derived from equation (15) for (a) estuarine, (b) fjord, (c) coastal, and (d) oceanic waters.

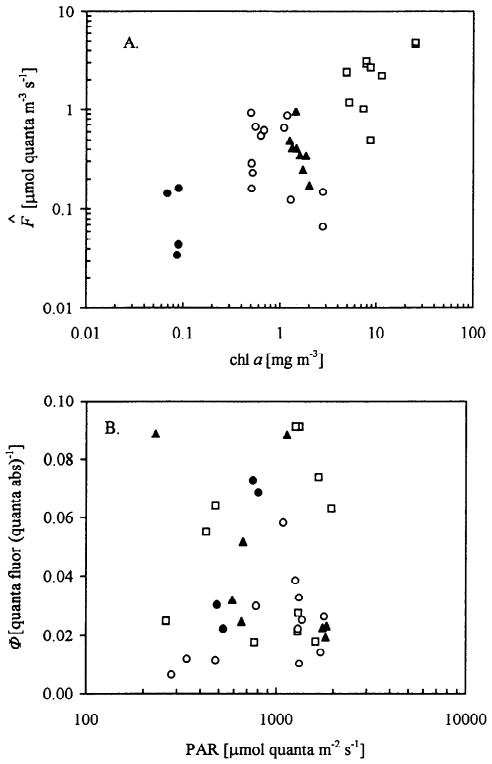

Figure 8. (a) Spectrally integrated (660 to 730 nm) volume fluorescence $\hat{F}$ versus chl a concentration for oceanic (solid circles), coastal (open circles), fjordal (solid triangles), and estuarine (open squares) waters. (b) Fluorescence quantum yield Φ versus spectrally averaged (400 to 700 nm) incident irradiance, photosynthetically available radiation (PAR). Symbols are same as in Figure 8a.

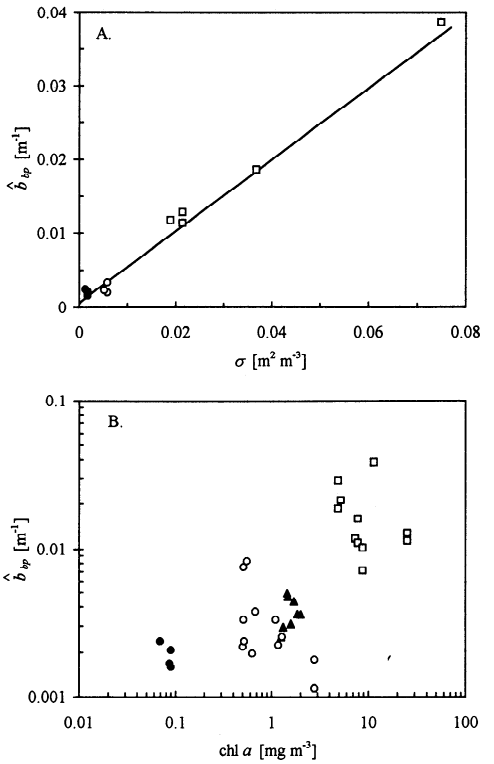

Figure 9. Estimated particle backscattering coefficients $\hat{b}_{bp}$ versus (a) total particle cross section σ and (b) chl a concentration. Symbols are same as in Figure 8a.

of backscattering than was chl a concentration (ρ = 0.47, n = 35, Figure 9B). It is noteworthy that the relationship between $\hat{b}_{bp}$ and chl a concentration exhibits significantly more scatter on log-transformed axes than does the relationship between $\hat{b}_{bp}$ and σ on linear axes.

5.4. Sensitivity Analysis

The magnitude of the M_i and M_j coefficients derived from the regression of (14) and the resulting spectral shape of $\hat{R}(\lambda, z_{0-})$ depend upon the definition of the basis vectors. However, the estimated phytoplankton and tripton/gelbstoff absorption and particle backscattering coefficients exhibited less than a factor of 2 variability (Table 2) even under extreme variations in the shape of the basis vector. The relatively large variations in the M coefficients due to varying $\mathbf{a}_\phi(\lambda)$ resulted from the *D. salina* and *Synechococcus* sp. absorption basis vectors. The pigment compositions of these pure cultures are not representative of the general phytoplankton populations found in situ, although representatives of these groups are found within naturally occurring populations. In some cases, the regression would not even converge with one or the other of these two spectra used as the basis vector. If these two spectra were removed from the sensitivity analysis, the resulting percent cv derived from using the remaining three phytoplankton basis vectors (Figure 1a) were significantly reduced, although the largest percent cv was always observed in the estuarine water cases.

Variations in the exponential slope of the tripton/gelbstoff absorption basis vector resulted in slightly lower percent cv in the estimated M coefficients, and these values were reduced by excluding the two extreme exponential slope values (S = 0.009 and 0.02). It should be noted, however, that a value of S = 0.02 used for the estuarine samples resulted in more accurate estimates of phytoplankton absorption coefficients due to the extremely high gelbstoff absorption.

Table 2. Results of Sensitivity Analysis for Equation (14): The Effect of Changes in the Basis Vectors on Estimated Phytoplankton $\hat{a}_\phi$ and Tripton/Gelbstoff $\hat{a}_{tg}$ Absorption and Particle Backscattering $\hat{b}_{bp}$ Coefficients

Estimated Coefficient	Varied Basis Vector	Environment			
		Estuarine	Fjord	Coastal	Oceanic
$\hat{a}_\phi$	$\mathbf{a}_\phi$	94 (47)	nd	38 (34)	43 (28)
	$\mathbf{a}_{tg}$	58 (49)	82 (72)	42 (39)	41 (34)
	$\mathbf{b}_{b2}$	50 (30)	27 (23)	18 (10)	38 (22)
$\hat{a}_{tg}$	$\mathbf{a}_\phi$	37 (12)	16 (11)	26 (15)	18 (16)
	$\mathbf{a}_{tg}$	34 (23)	42 (30)	26 (17)	20 (16)
	$\mathbf{b}_{b2}$	53 (40)	76 (29)	81 (52)	62 (57)
$\hat{b}_{bp}$	$\mathbf{a}_\phi$	40 (5)	10 (8)	14 (12)	8 (5)
	$\mathbf{a}_{tg}$	26 (19)	15 (9)	7 (4)	1 (1)
	$\mathbf{b}_{b2}$	39 (18)	27 (33)	33 (21)	20 (6)

Averaged coefficients of variations, expressed as percent coefficients of variation (cv), were determined for each environment. Numbers in parentheses are percent cv with the two most extreme basis vectors removed; i.e., for $\mathbf{a}_\phi$, *D. salina* and *Synechococcus* sp.; for $\mathbf{a}_{tg}$, S = 0.02 and 0.009; and for $\mathbf{b}_{b2}$, Y = 0.0 and 1.2. For fjord $\mathbf{a}_\phi$, nd indicates not determinable; model would not converge with any other $\mathbf{a}_\phi$.

The standard basis vector for the wavelength-dependent particle backscattering $\mathbf{b}_{b2}$ was assumed to have a λ^{-Y} dependence, where $Y = 1$ was not variable. In the sensitivity analysis, Y was defined as a regression coefficient and allowed to vary. However, the regression requires a initial guess for all coefficients. The values M_{ϕ}, M_{tg}, M_{b1}, and M_{b2} obtained after convergence were not a function of the value of the initial guesses. However, the value for Y obtained after convergence was strongly dependent upon the initial guess. The initial values for $Y = 0$, 0.5, 0.75, 1.0, 1.1, and 1.2 were used in the sensitivity analysis. In all cases, the model converged with resulting Y coefficients varying by <5% from the initial value. Again, exclusion of the extreme basis vectors with $Y = 0$ and $Y = 1.2$ reduced the percent cv.

6. Discussion

Reflectance spectra were obtained from a diverse set of optical domains. Over this large range of optical domains, phytoplankton spectral absorption coefficients were accurately estimated using the inverse reflectance model. The assumptions of the model were (1) that the approximation for in situ reflectance in terms of measurable quantities in (6) was valid, (2) that all the components responsible for absorption and backscattering were identified, and (3) that the basis vectors were accurately defined. The observed coherence between the in situ and model reconstructed reflectance spectra, examples of which are shown in Figure 4, suggest that the assumptions were valid. It is noteworthy that the basis vectors used in this paper were defined from previously published data and theory and thus were not optimized for the diverse optical conditions encountered with this data set. Although the accuracy of the model could be improved with regionally defined basis vectors for phytoplankton and tripton/gelbstoff absorption, the model appears to be quite robust and seamless for all types of waters. The in situ measurement of backscattering spectra is, as yet, minimal [*Bricaud et al.*, 1995] and is of utmost importance for understanding both in situ and remote sensing reflectance. The backscattering basis vectors are the least tested of the basis vectors used in this paper, and the model predictability will be improved most by the inclusion of realistic backscattering spectra.

The estimation of spectral phytoplankton absorption coefficients from remote measurements is important for predicting both the distribution and primary production of phytoplankton from remote sensing reflectance. This reflectance model results in estimates of the magnitude and spectral shape of phytoplankton absorption within 35% for most environments. The phytoplankton absorption coefficients for the estuarine environment, which was characterized by extremely large tripton/gelbstoff absorption coefficients not typical of most ocean waters, were always overestimated. The model results for the estuarine case were very sensitive to the selection of basis vectors; thus regionally defined basis vectors should improve the prediction in these waters. The model contains no input for pigment packaging variations associated with photoadaptation, per se. However, the second-order estimated phytoplankton absorption coefficients will incorporate those spectral variations associated with packaging, pigment composition, or detrital pigments that are significant enough to alter the shape of the reflectance spectrum (e.g., as was the case with detrital pigments in Figure 6b).

Phytoplankton absorption coefficients are more directly tied to reflectance spectra via (6) than are bulk measurements of phytoplankton such as chl *a* concentration. The estimation of chl *a* from reflectance ratios is primarily determined by the spectral phytoplankton absorption coefficient and secondarily by the empirical correlation between phytoplankton absorption coefficient and chl *a* concentration. The links between the reflectance, absorption, and chl *a* are what determined the empirically derived coefficients in the standard chlorophyll algorithm for the coastal zone color scanner [*Gordon and Morel*, 1983]. Thus the primary product of an in situ or remote sensing reflectance model is actually a measure of phytoplankton absorption. Chl *a* concentrations, if desired, can be subsequently estimated more accurately using regionally defined chl *a*-specific phytoplankton absorption coefficients.

The ability to extract solar-stimulated chl *a* fluorescence spectra from irradiance reflectance or upward irradiance or radiance may provide an independent measure of phytoplankton biomass [*Neville and Gower*, 1977; *Sugihara et al.*, 1986], physiological status [*Falkowski and Kiefer*, 1985], or photosynthetic rate [*Chamberlin et al.*, 1990]. Obtaining fluorescence values corrected for backscattering has previously been difficult. Most approaches have emphasized the estimation of background irradiance, radiance, or reflectance at wavelengths within the fluorescence band by assuming (1) a linear relationship between two signals measured on either side of the fluorescence signature, (2) a constant backscattering coefficient, or (3) a constant Gaussian shape to the fluorescence spectrum.

The modeled reflectance spectra derived from the forward equation (14) indicate that the nonfluorescence portion of reflectance does not linearly decrease over the fluorescence wave band, as was also predicted by the theoretical model of *Kishino et al.* [1986]. A linear decrease in reflectance would imply a linear decrease in the ratio of backscattering to absorption. Absorption by chl *a* in the fluorescence wave band negates that assumption. The reflectance model presented here incorporates variations in spectral shape of backscattering and absorption, resulting in the resolution of the spectral shape of the fluorescence emission spectra even at chl *a* concentrations <0.1 mg m^{-3}. While any differences between R and $\hat{R}$ are incorporated into the estimated fluorescence emission spectrum in the wave band 650 to 730 nm, it should be noted that the reflectance is dominated by the absorption and backscattering by water and the absorption by phytoplankton. The water contribution in this wave band is relatively constant and well constrained. The contribution to phytoplankton absorption by accessory pigments is minimal, and packaging effects are much reduced compared with the blue region of the spectrum. Thus the errors in $\hat{R}$ in this wave band will minimally affect $\hat{F}$.

The in situ fluorescence spectra derived from this model were not purely Gaussian nor were the fluorescence maxima always at 683 nm. The shift in maximal fluorescence and the variations in fluorescence spectral shape were also observed by *Gordon* [1979] using radiative transfer theory with measurements from *Morel and Prieur* [1977]. *Ahn et al.* [1992] observed variations in the shape of the chl *a* fluorescence

emission spectra for a variety of phytoplankton species, most notably for those containing phycobilipigments and perhaps related to variations in pigment-protein complexes in photosystem II [*Govindje et al.*, 1979]. Variations in the peak height to peak width, also called spectral whitening, and shifts in the wavelength of maximal fluorescence may also be due to reabsorption of the fluoresced photons by chl *a* [*Collins et al.*, 1985]. This phenomenon would be especially apparent under conditions of high chl *a* concentrations such as was observed in Puget Sound where the associated fluorescent emission spectra were very broad. The model presented here does not account for anomalous dispersion of backscattering about absorption features. It has been shown that such a process about the red chl *a* absorption peak can result in enhanced backscattering coefficients in the wave band associated with fluorescence and may also account for some of the variability in the estimated fluorescence emission [*Zaneveld and Kitchen*, this issue].

The relationship between fluorescence and chl *a* concentration has been observed many times. It is interesting to note, however, that the linear relationship is only observed in this data set over the nearly 4 orders of magnitude dynamic range of chl *a* concentrations, demonstrating that volume natural fluorescence is only a gross indicator of chl *a* concentrations. Regionally, the volume natural fluorescence and chl *a* exhibited no correlation (estuarine and oceanic waters) or even slightly negative correlation (coastal and fjord waters). The variability in the fluorescence chl *a* regression is probably a function of surface irradiance. The quantum yields are submaximal at both low surface irradiance (subinhibiting irradiances) and high surface irradiance (inhibiting irradiances) (Figure 8b). The calculated values for fluorescence quantum yield were of the same magnitudes as those determined by *Chamberlin et al.* [1990] at high irradiances. However, our values tended to be larger, possibly because our measurements (1) were taken at the surface at local noon, while their measurements were taken along vertical profiles; (2) were integrated over the full range of fluorescence emission; (3) and incorporated a more accurate correction for backscattered red light. Within each environment the maximal quantum yield occurred at approximately 1000 μmol quanta m^2 s^{-1} and decreased at higher surface irradiances, perhaps due to photoinhibition effects on fluorescence quenching [*Neale*, 1987; *Cullen et al.*, 1994]. This is similar to the value of approximately 750 μmol quanta m^2 s^{-1} observed by *Kiefer et al.* [1989] in the western South Pacific gyre.

Fluorescence by chromoproteins or dissolved organic matter (gelbstoff) was not included in this model. There is evidence suggesting that the effect may be negligible in most oceanic waters. In organic-rich coastal waters the magnitude of this signal was as high as 8% of the total reflectance [*Hawes et al.*, 1992]. In fresh waters, however, the effect may be quite significant; a reflectance spectrum obtained from Lake Washington did appear to be contaminated by fluorescence due to both phycoerithrin and dissolved organic matter (14% and 30% of the measured reflectance, respectively [*Culver and Perry*, 1994]). As more information is gained concerning the fluorescence spectral shape and efficiency by these other components, these signals could be resolved similarly to that of chl *a* fluorescence.

Modeled particle backscattering coefficients ranged over 3 orders of magnitude (Table 1). Although there were no direct measurements for comparison, it was expected that the particle backscattering coefficient would be linearly related to the total optical cross section of the in situ particles. For large and polydisperse populations of particles the optical and geometrical cross sections are directly related. A strong linear relationship between the particle backscattering and the geometric cross section was found for three environments where particle information was collected. It is noteworthy that these locations represented the extremes in absorption and reflectance spectral ranges. An important future test would be to measure backscattering spectra independently for comparison with estimated spectral coefficients. Also noteworthy is the poor correlation between the derived backscattering coefficients and chl *a* concentration within each environment. Although a stronger correlation has been observed in some regions [*Morel*, 1988], it is likely an artifact of the covariation between particles and chl *a* [see *Kitchen and Zaneveld*, 1990].

The vertical scale on which the present measurements were made does not allow for resolution of vertical variability in the absorption and backscattering coefficients. Certainly, significant vertical structure in these coefficients would be manifested in the measured reflectance spectrum [*Zaneveld*, 1982]. The absorption and backscattering coefficients derived from the model represent weighted average values for the near-surface waters. Errors between modeled and measured absorption and backscattering coefficients may arise in highly stratified surface waters if the measured coefficients are not properly scaled by optical depth.

The application of this model to the remote sensing of ocean color is the next logical step for assessing the utility of this approach. The water-leaving radiance measured by satellite-based sensors can be approximated from the in-water reflectance by the relationship between (5) and (6). The model should be tested directly on true remote sensing reflectance, the ratio of upward radiance to downward irradiance, as opposed to the irradiance reflectance used here. Such a test would allow direct comparison of L_u with the radiance signal detected by satellite or airborne sensors. It would also remove the Q factor from the expression, as (5) and not (6) is used to relate reflectance to the inherent optical properties. As has been shown by *Zaneveld* [this issue], constraints on the shape factors f_b and f_L are more rigorous than those on Q. This will serve to remove the passage of errors from Q to the estimates of phytoplankton absorption, chl *a* fluorescence, and particle backscattering.

At present, it is difficult to obtain absolute radiances from ocean color sensors; hence it is necessary to calculate normalized water-leaving radiances. The reflectance model presented here, applied to normalized radiance measurements, would result in estimations of the relative proportions of each component. The magnitudes of water absorption and backscattering coefficients are known, and thus the absolute concentration of the other components could be calculated relative to the water optical coefficients. Application of this approach to a multispectral radiance sensor such as the sea-viewing wide field-of-view sensor (Sea WiFS) would result in multispectral phytoplankton absorption coefficients for use in bio-optical primary production models or for use in resolving some taxonomic information, based upon pigment absorption features, from space.

Notation

A effective area of the filter, cm^2.
$a_x(\lambda)$ spectral absorption coefficients, where subscript $x = T$, ϕ, g, t, tg, or w, for total, phytoplankton, gelbstoff, tripton, tripton plus gelbstoff, or water, respectively, m^{-1}.
$\hat{a}_\phi(\lambda)$ first-order modeled spectral phytoplankton absorption coefficients, m^{-1}.
$\mathring{a}_\phi(\lambda)$ second-order modeled spectral phytoplankton absorption coefficient, m^{-1}.
$\mathbf{a}_i(\lambda)$ absorption basis vector for component $i = \phi$ or tg, dimensionless.
$a^*_\phi(\lambda)$ chl a-specific spectral phytoplankton absorption coefficient, m^2 (mg chl a)$^{-1}$.
b_f forward scattering coefficient averaged over PAR, m^{-1}.
$b_{bx}(\lambda)$; b_{bx} spectral backscattering coefficient; backscattering coefficient averaged over PAR, where subscript $x = T$, p, or w for total, particle, or water, respectively, m^{-1}.
$\hat{b}_{bj}(\lambda)$; $\hat{b}_{bj}$ modeled spectral backscattering coefficient; modeled backscattering coefficient averaged over PAR for component j, where $j = p$, 1, or 2 for particle backscattering, wavelength-independent backscattering, or wavelength-dependent backscattering, respectively, m^{-1}.
$\mathbf{b}_{bj}(\lambda)$ backscattering basis vector for component j, where $j = 1$ or 2, for wavelength-independent backscattering or wavelength-dependent backscattering, respectively, dimensionless.
c beam attenuation coefficient, m^{-1}.
chl a chlorophyll a concentration, mg m^{-3}.
d equivalent spherical diameter of particles, μm.
E_d; $\hat{E}_d$ measured; modeled downward quantum vector irradiance, μmol quanta m^2 s^{-1}.
E_u; $\hat{E}_u$ measured; modeled upward quantum vector irradiance, μmol quanta m^{-2} s^{-1}.
$\hat{E}_{ouF}$ estimated upward quantum scalar irradiance of solar-stimulated chl a fluorescence, μmol quanta m^{-2} s^{-1}.
ESD equivalent spherical diameter, μm.
$\hat{F}$ estimated solar-stimulated volume chl a fluorescence, μmol quanta m^{-3} s^{-1}.
G coefficient scaling reflectance to the ratio of backscattering to absorption.
f_b shape factor for reflectance, the integrated backscattered downward radiance scaled to the backscattered downward scalar irradiance, dimensionless.
f_L shape factors for reflectance, the integrated forward scattered upward radiance scaled to the total forward scattered radiance, dimensionless.
k attenuation for nadir radiance, m^{-1}.
k_d attenuation coefficient for downward irradiance, m^{-1}.
k_u attenuation coefficient for upward irradiance, m^{-1}.
L optical path length, cm^{-1}.
L_u upward radiance, μmol quanta m^{-2} s^{-1} sr^{-1}.
M_i, M_j magnitude of component optical coefficients, where subscript $i = \phi$ or tg for absorption, and $j = b1$ or $b2$ for backscattering, m^{-1}.
N particle concentration, particles mL^{-1}.
OD optical density, dimensionless.
PAR photosynthetically available radiation (400–700 nm), μmol quanta m^{-2} s^{-1}.
Q ratio of upward irradiance to upward radiance, sr^{-1}.
$R(\lambda)$ in situ spectral irradiance reflectance, dimensionless.
$\hat{R}(\lambda)$ estimated spectral irradiance reflectance, dimensionless.
$\hat{R}_F(\lambda)$ estimated spectral irradiance reflectance due to solar-stimulated chl a fluorescence, dimensionless.
S exponential slope of the tripton/gelbstoff basis vector, nm^{-1}.
V volume filtered, mL.
Y coefficient defining wavelength dependence of particle backscattering basis vector (i.e., λ^{-Y}), dimensionless.
z depth, m.
z_{0+} depth just above air/sea interface, m.
z_{0-} depth just below air/sea interface, m.
β path length amplification factor for filter pad absorption calculation, dimensionless.
Φ fluorescence quantum yield, quanta fluoresced (quanta absorbed)$^{-1}$.
λ wavelength, nm.
λ_F chl a fluorescence wave band (660–730 nm), nm.
$\Delta\lambda_{\min}$ 30-nm wave band of minimal irradiance attenuation in near-surface waters, nm.
$\bar{\mu}_x$ average cosine, where subscript $x = o$, d, u, and ∞ for incident, downward, upward, and asymptotic irradiance fields, respectively, dimensionless.
σ total geometric cross-sectional area for particles, μm^2 mL^{-1}.
τ transmission across the air/sea interface, dimensionless.

Acknowledgments. Tim Cowles and John Marra kindly provided cruise opportunities on the R/V *Wecoma* to the MultiTracers Transect (NSF-sponsored Laser91) and the R/V *Endeavor* to the Gulf of Maine (ONR-sponsored Marine Light Mixed Layer), respectively. We thank Mónica Orellana and Mary Kay Talbot for invaluable field assistance; Jody Deming for the use of her Coulter counter and Richard Davis, Russ Desiderio, Jim Kitchen, Robert Maffione, Norman McCormick, Scott Pegau, Charlie Yentsch, and Ron Zaneveld for helpful comments on the manuscript. John Adams first suggested the application of terrestrial reflectance mixture models to oceanic reflectance. André Morel provided many useful discussions in the early stages of reflectance modeling. This work was funded by a fellowship from the NASA Graduate Student Researchers Program grant NGT-50681 (C. S. Roesler) and the Office of Naval Research grants N00014-93I-0150 (C. S. Roesler) and N00014-90J-1091 (M. J. Perry). University of Washington School of Oceanography contribution 2117.

References

Aas, E., Two-stream irradiance model for deep waters, *Appl. Opt.*, *26*, 2095–2101, 1987.

Ackleson, S. G., W. M. Balch, and P. M. Holligan, The response of water-leaving radiance to particulate calcite and chlorophyll *a* concentration: A model for Gulf of Maine coccolithophore blooms, *J. Geophys. Res.*, *99*, 7483–7499, 1994.

Adams, J. B., M. O. Smith, and P. E. Johnson, Spectral mixture modeling: A new analysis of rock and soil types at the Viking Lander 1 site, *J. Geophys. Res.*, *91*, 8908–8112, 1986.

Adams, J. B., M. O. Smith, and A. R. Gillespie, Imaging spectroscopy: Interpretation based on spectral mixture analysis, in *Remote Geochemical Analysis: Elemental and Mineralogical Composition*, edited by C. M. Pieters and P. Englert, pp. 145–166, Cambridge University Press, New York, 1993.

Ahn, Y. H., A. Bricaud, and A. Morel, Light backscattering efficiency and related properties of some phytoplankters, *Deep Sea Res., Part I*, *39*, 1835–1855, 1992.

Austin, R. W., Inherent spectral radiance signatures of the ocean surface, in Ocean Color Analysis, *Ref. Publ. 74-10*, Scripps Inst. of Oceanogr., La Jolla, Calif., 1974.

Betzer, P. R., et al., Long-range transport of giant mineral aerosol particles, *Nature*, *336*, 568–571, 1988.

Bidigare, R. R., J. H. Morrow, and D. A. Kiefer, Derivative analysis of spectral absorption by photosynthetic pigments in the western Sargasso Sea, *J. Mar. Res.*, *47*, 323–341, 1989.

Bidigare, R. R., B. B. Prézelin, and R. C. Smith, Bio-optical models and the problems of scaling, in *Primary Productivity and Biogeochemical Cycles in the Sea*, edited by P. G. Falkowski and A. D. Woodhead, pp. 1175–212, Plenum, New York, 1992.

Bishop, J. K. B., The correction and suspended particulate matter calibration of Sea Tech transmissometer data, *Deep Sea Res., Part A*, *33*, 121–134, 1986.

Bricaud, A., and A. Morel, Light attenuation and scattering by phytoplanktonic cells: A theoretical modeling, *Appl. Opt.*, *25*, 571–580, 1986.

Bricaud, A., A. Bedhomme, and A. Morel, Optical properties of diverse phytoplanktonic species: Experimental results and theoretical interpretation, *J. Plankton Res.*, *10*, 851–873, 1988.

Bricaud, A., C. S. Roesler, and J. R. V. Zaneveld, *In situ* attenuation, absorption, and backscattering properties of oceanic and coastal waters off Oregon, *Limnol. Oceanogr.*, in press, 1995.

Carder, K. L., R. G. Steward, G. R. Harvey, and P. B. Ortner, Marine humic and fulvic acids: Their effects on remote sensing of ocean chlorophyll, *Limnol. Oceanogr.*, *34*, 68–8, 1989.

Chamberlin, W. S., and J. Marra, Estimation of photosynthetic rate from measurements of natural fluorescence: Analysis of the effects of light and temperature, *Deep Sea Res., Part I*, *39*, 1695–1706, 1992.

Chamberlin, W. S., C. R. Booth, D. A. Kiefer, J. H. Morrow, and R. C. Murphy, Evidence for a simple relationship between natural fluorescence, photosynthesis and chlorophyll in the sea, *Deep Sea Res., Part A*, *37*, 951–973, 1990.

Collins, D., D. A. Kiefer, J. B. SooHoo, and I. S. McDermid, The role of reabsorption in the spectral distribution of phytoplankton fluorescence emission, *Deep Sea Res., Part A*, *32*, 983–1003, 1985.

Cullen, J. J., P. J. Neale, R. F. Davis, and R. S. Lean, Ultraviolet radiation, vertical mixing, and primary productivity in the Antarctic (abstract), *Eos Trans. AGU*, *75*(3), Ocean Sciences Meeting suppl., 200, 1994.

Culver, M. E., and M. J. Perry, Detection of phycoerythrin fluorescence in upwelling irradiance spectra (abstract), *Eos Trans. AGU*, *75*(3), Ocean Sciences Meeting suppl., 233, 1994.

Falkowski, P. G., and D. A. Kiefer, Chlorophyll *a* fluorescence and phytoplankton: Relationship to photosynthesis and biomass, *J. Plankton Res.*, *7*, 715–731, 1985.

Gordon, H. R., Diffuse reflectance of the ocean: The theory of its augmentation by chlorophyll *a* fluorescence at 685 nm, *Appl. Opt.*, *18*, 1161–1166, 1979.

Gordon, H. R., and A. Morel, *Remote Assessment of Ocean Color for Interpretation of Satellite Visible Imagery: A Review*, 114 pp., Springer-Verlag, New York, 1983.

Gordon, H. R., O. B. Brown, and M. M. Jacobs, Computed relationships between the inherent and apparent optical properties of a flat homogeneous ocean, *Appl. Opt.*, *14*, 417–427, 1975.

Gordon, H. R., O. B. Brown, R. H. Evans, J. W. Brown, R. C. Smith, K. S. Baker, and D. K. Clark, A semianalytic radiance model of ocean color, *J. Geophys. Res.*, *93*, 10,909–10,924, 1988.

Govindje, D. Wong, B. B. Prézelin, and B. M. Sweeney, Chlorophyll *a* fluorescence of *Gonyaulax polyedra* frown on a light-dark cycle after transfer to a constant light, *Photochem. Photobiol.*, *30*, 405–411, 1979.

Hawes, S. K., K. L. Carder, and G. R. Harvey, Quantum fluorescence efficiencies of fulvic and humic acids: Effects on ocean color and fluorometric detection, Ocean Optics 11, *Proc. SPIE Int. Soc. Opt. Eng.*, *1750*, 212–223, 1992.

Heath, M. R., K. Richardson, and T. KiØrboe, Optical assessment of phytoplankton nutrient depletion, *J. Plankton Res.*, *12*, 381–396, 1990.

Holm-Hansen, O., C. J. Lorenzen, R. W. Holmes, and J. D. Strickland, Fluorometric determination of chlorophyll, *J. Cons. Cons. Int. Explor. Mer*, *30*, 3–15, 1965.

Johnson, P. E., M. O. Smith, S. Taylor-George, and J. B. Adams, A semiempirical method for analysis of the reflectance spectra of binary mineral mixtures, *J. Geophys. Res.*, *88*, 3557–3561, 1983.

Johnson, P. E., R. B. Singer, M. O. Smith, and J. B. Adams, Simple algorithms for remote determination of mineral abundances and particle sizes from reflectance spectra, *J. Geophys. Res.*, *97*, 2649–2658, 1992.

Kiefer, D. A., and R. A. Reynolds, Advances in understanding phytoplankton fluorescence and photosynthesis, in *Primary Productivity and Biogeochemical Cycles in the Sea*, edited by P. G. Falkowski and A. D. Woodhead, pp. 155–174, Plenum, New York, 1992.

Kiefer, D. A., and J. B. SooHoo, Spectral absorption by marine particles of coastal waters of Baja California, *Limnol. Oceanogr.*, *27*, 492–499, 1982.

Kiefer, D. A., W. S. Chamberlin, and C. R. Booth, Natural fluorescence of chlorophyll *a*: Relationship to photosynthesis and chlorophyll concentration in the western South Pacific gyre, *Limnol. Oceanogr.*, *34*, 868–881, 1989.

Kirk, J. T. O., Spectral absorption properties of natural waters: Contribution of the soluble and particulate fractions to light absorption in some inland waters in south-eastern Australia, *Aust. J. Mar. Freshwater Res.*, *31*, 287–296, 1980.

Kirk, J. T. O., A Monte Carlo study of the nature of the underwater light field in, and the relationships between optical properties of, turbid yellow waters, Australia, *Aust. J. Mar. Freshwater Res.*, *32*, 517–532, 1981.

Kirk, J. T. O., Dependence of relationship between inherent and apparent optical properties of water on solar altitude, *Limnol. Oceanogr.*, *29*, 350–356, 1984.

Kishino, M., C. R. Booth, and N. Okami, Underwater radiant energy absorbed by phytoplankton, detritus, dissolved organic matter, and pure water, *Limnol. Oceanogr.*, *29*, 340–349, 1984a.

Kishino, M., S. Sugihara, and N. Okami, Influence of fluorescence of chlorophyll *a* on underwater upward irradiance spectrum, *La Mer*, *22*, 224–232, 1984b.

Kishino, M., M. Takahashi, N. Okami, and S. Ichimura, Estimation of the spectral absorption coefficients of phytoplankton in the sea, *Bull. Mar. Sci.*, *37*, 634–642, 1985.

Kishino, M., S. Sugihara, and N. Okami, Theoretical analysis of the *in situ* fluorescence of chlorophyll *a* on the underwater spectral irradiance, *La Mer*, *24*, 130–138, 1986.

Kitchen, J. C., and H. Pak, Observations of natural fluorescence with an underwater radiometer, *J. Oceanogr. Soc. Jpn.*, *43*, 356–362, 1987.

Kitchen, J. C., and J. R. V. Zaneveld, On the noncorrelation of the vertical structure of light scattering and chlorophyll *a* in case I waters, *J. Geophys. Res.*, *95*, 20,237–20,246, 1990.

Maffione, R. A., D. R. Dana, and R. C. Honey, Instrument for underwater measurement of optical backscatter, *Proc. SPIE Int. Soc. Opt. Eng.*, *1537*, 173–184, 1991.

McCormick, N., Asymptotic optical attenuation, *Limnol. Oceanogr.*, *37*, 1570–1578, 1992.

Mitchell, B. G., Algorithms for determining the absorption coefficients of aquatic particulates using the quantitative filter technique (QFT), *Proc. SPIE Int. Soc. Opt. Eng.*, *1302*, 137–148, 1990.

Mitchell, B. G., and D. A. Kiefer, Determination of absorption and fluorescence excitation spectra for phytoplankton, in *Marine*

Phytoplankton and Productivity, edited by O. Holm-Hansen, pp. 157–169, Springer-Verlag, New York, 1984.

Mitchell, B. G., and D. A. Kiefer, Chlorophyll a specific absorption and fluorescence excitation spectra for light-limited phytoplankton, *Deep Sea Res., Part A*, *35*, 639–663, 1988.

Moore, C., J. R. V. Zaneveld, and J. C. Kitchen, Preliminary results from an *in situ* spectral absorption meter, Ocean Optics 11, *Proc. SPIE Int. Soc. Opt. Eng.*, *1750*, 330–337, 1992.

Morel, A., Optical modeling of the upper ocean in relation to its biogenous matter content (case I waters), *J. Geophys. Res.*, *93*, 10,749–10,768, 1988.

Morel, A., and Y. H. Ahn, Optical efficiency factors of free living marine bacteria: Influence of bacterioplankton upon the optical properties and particulate organic carbon in the ocean waters, *J. Mar. Res.*, *48*, 145–175, 1990.

Morel, A., and Y. H. Ahn, Optics of heterotrophic nanoflagellates and ciliates: A tentative assessment of their scattering role in oceanic waters compared to those of bacterial and algal cells, *J. Mar. Res.*, *49*, 177–202, 1991.

Morel, A., and L. Prieur, Analysis of variations in ocean color, *Limnol. Oceanogr.*, *22*, 709–722, 1977.

Neale, P. J., Algal photoinhibition and photosynthesis in the aquatic environment, in *Photoinhibition*, edited by D. J. Kyle, C. B. Osmond, and C. J. Arntzen, pp. 39–65, Elsevier, New York, 1987.

Neori, A., O. Holm-Hansen, B. G. Mitchell, and D. A. Kiefer, Photoadaptation in marine phytoplankton, *Plant Physiol.*, *76*, 518–524, 1984.

Neville, R. A., and J. F. R. Gower, Passive remote sensing of phytoplankton via chlorophyll *a* fluorescence, *J. Geophys. Res.*, *82*, 3487–3493, 1977.

Petzold, T. J., *Volume Scattering Functions for Selected Ocean Waters*, Scripps Institution of Oceanography, La Jolla, Calif., 1972.

Press, W. H., B. P. Flannery, S. A. Teukolsky, and W. T. Vetterling, *Numerical Recipes, The Art of Scientific Computing*, Cambridge University Press, New York, 1986.

Prieur, L., and S. Sathyendranath, An optical classification of coastal and oceanic waters based on the specific spectral absorption curves of phytoplankton pigments, dissolved organic matter, and other particulate materials, *Limnol. Oceanogr.*, *26*, 671–689, 1981.

Roesler, C. S., The determination of *in situ* phytoplankton spectral absorption coefficients: Direct measurements, modeled estimates, and applications to bio-optical modeling, Ph.D. thesis, Univ. of Wash., Seattle, 1992.

Roesler, C. S., and J. R. V. Zaneveld, High resolution vertical profiles of spectral absorption, attenuation, and scattering coefficients in highly stratified waters, Ocean Optics 12, *Proc. SPIE Int. Soc. Opt. Eng.*, *2258*, 309–319, 1994.

Roesler, C. S., M. J. Perry, and K. L. Carder, Modeling *in situ* phytoplankton absorption from total absorption spectra in productive inland marine waters, *Limnol. Oceanogr.*, *34*, 1510–1523, 1989.

Sathyendranath, S., L. Lazarra, and L. Prieur, Variations in the spectral values of specific absorption of phytoplankton, *Limnol. Oceanogr.*, *32*, 403–415, 1987.

Shifrin, K. S., *Physical Optics of Ocean Water*, American Institute of Physics, College Park, Md., 1988.

Smith, R. C., and K. S. Baker, Optical properties of the clearest natural waters, *Appl. Opt.*, *20*, 177–184, 1981.

Stegmann, P. M., M. R. Lewis, C. O. Davis, and J. J. Cullen, Primary production estimates from recordings of solar-stimulated fluorescence in the equatorial Pacific at 150°W, *J. Geophys. Res.*, *97*, 626–638, 1992.

Stramski, D., and D. Kiefer, Light scattering by microorganisms in the ocean, *Prog. Oceanogr.*, *28*, 343–383, 1991.

Stramski, D., and A. Morel, Optical properties of photosynthetic picoplankton in different physiological states as affected by growth irradiance, *Deep Sea Res., Part A*, *37*, 245–266, 1990.

Sugihara, S., M. Kishino, and N. Okami, Estimation of water quality parameters from irradiance reflectance using optical models, *J. Oceanogr. Soc. Jpn.*, *41*, 399–406, 1985.

Sugihara, S., M. Kishino, and N. Okami, Estimation of chlorophyll concentration from the specific fluorescence at 685 nm in the upward irradiance just below the sea surface, *J. Oceanogr. Soc. Jpn.*, *42*, 99–105, 1986.

Topliss, B. J., Optical measurements in the Sargasso Sea: Solar stimulated chlorophyll fluorescence, *Oceanol. Acta*, *8*, 263–270, 1985.

Yentsch, C. S., Measurement of visible light absorption by particulate matter in the ocean, *Limnol. Oceanogr.*, *7*, 207–217, 1962.

Yentsch, C. S., and D. A. Phinney, A bridge between ocean optics and microbial ecology, *Limnol. Oceanogr.*, *34*, 1698–1709, 1989.

Yentsch, C. S., and D. A. Phinney, Spectral diffuse attenuation of phytoplankton measured by the filter pad technique—Are we on the right track?, *Proc. SPIE Int. Soc. Opt. Eng.*, *1750*, 180–186, 1992.

Zaneveld, J. R. V., Remotely sensed reflectance and its dependence on vertical structure: A theoretical derivation, *Appl. Optics*, *21*, 4146–4150, 1982.

Zaneveld, J. R. V., A theoretical derivation of the dependence of the remotely sensed reflectance of the ocean on the inherent optical properties, *J. Geophys. Res.*, this issue.

Zaneveld, J. R. V., and J. C. Kitchen, The variation in the inherent optical properties of phytoplankton near an absorption peak as determined by various models of cell structure, *J. Geophys. Res.*, this issue.

Zaneveld, J. R. V., J. C. Kitchen, A. Bricaud, and C. Moore, Analysis of *in situ* spectral absorption meter data, Ocean Optics 11, *Proc. SPIE Int. Soc. Opt. Eng.*, *1750*, 180–186, 1992.

M. J. Perry, School of Oceanography, WB-10, University of Washington, Seattle, WA 98195.

C. S. Roesler, Department of Marine Sciences, University of Connecticut, 1084 Shennecossett Road, Groton, CT 06340.

(Received April 25, 1994; revised December 2, 1994; accepted December 22, 1994.)